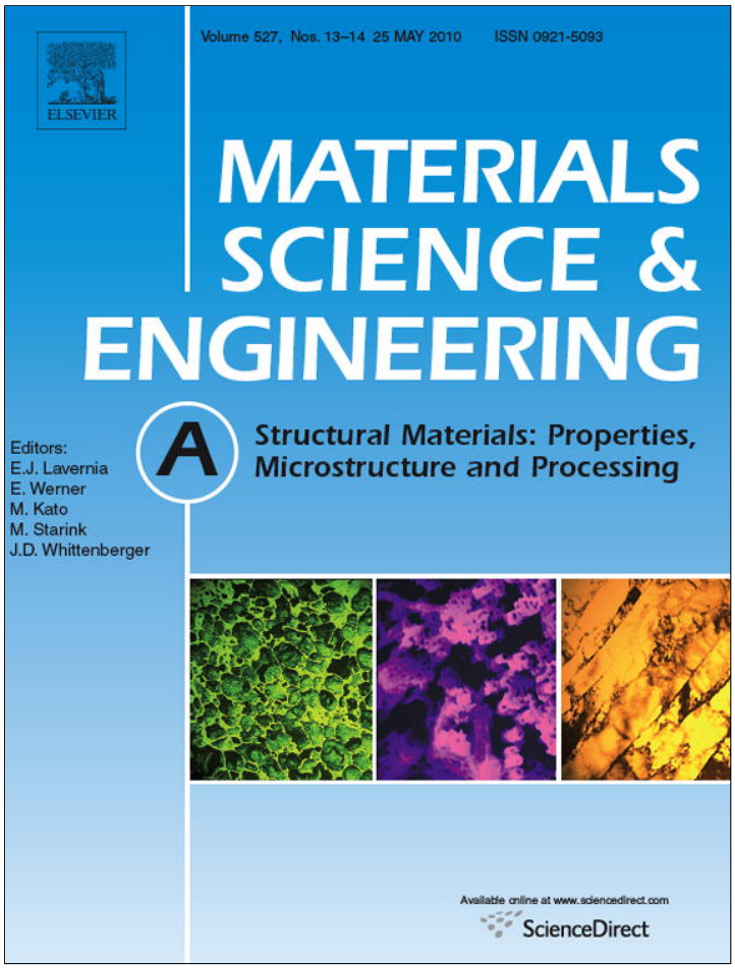

Materials Science and Engineering A 527 (2010) 3271–3278

Contents lists available at ScienceDirect

Materials Science and Engineering A

journal homepage: www.elsevier.com/locate/msea

Plastic anisotropy of ultrafine grained aluminium alloys produced by accumulative roll bonding

B. Beausir[a,*], J. Scharnweber[a], J. Jaschinski[b], H.-G. Brokmeier[c], C.-G. Oertel[a], W. Skrotzki[a]

[a] Institut für Strukturphysik, Technische Universität Dresden, D-01062 Dresden, Germany
[b] Institut für Leichtbau und Kunststofftechnik, Technische Universität Dresden, D-01062 Dresden, Germany
[c] GKSS Forschungszentrum, Max-Planck-Straße, D-21494 Geesthacht, Germany

ARTICLE INFO

Article history:
Received 14 August 2009
Received in revised form 1 February 2010
Accepted 2 February 2010

Keywords:
Aluminium alloys
Accumulative roll bonding (ARB)
Texture
Mechanical anisotropy
Lankford parameter
Modelling

ABSTRACT

The plastic anisotropy of ultrafine grained aluminium alloys AA1050 and AA6016 produced by accumulative roll bonding (ARB) has been investigated by tensile deformation via the Lankford parameter. The average normal and planar anisotropies slightly increase (from 0.6 to 0.9) and decrease (from 0.6 to −0.7) as a function of ARB cycles, respectively. The global textures measured by neutron diffraction are used to simulate the Lankford and anisotropy parameters of the plates after 0, 2, 4, 6 and 8 ARB cycles with the help of the viscoplastic polycrystal self-consistent model. Simulation results are compared with those from experiment and discussed with regard to texture, strain rate sensitivity, grain shape and slip system activity.

1. Introduction

During recent years, bulk ultrafine grained (UFG) materials produced by severe plastic deformation (SPD) have received considerable scientific attention (see reviews [1,2]). Due to their significantly higher specific strength, UFG materials have a high light-weight construction potential for automobile and aircraft industry. From the technical point of view, accumulative roll bonding (ARB) [[3–5] and review [6]] is a highly promising SPD process because it incorporates the production of new UFG materials and because it can be integrated into existing industrial process chains without important modifications.

An important concern when producing bulk UFG materials by ARB is to achieve a reasonable homogeneous microstructure and texture using the smallest possible number of cycles. Indeed, shear components are introduced into the material during conventional rolling. One acting in the plane normal to rolling direction (RD) in normal direction (ND), mostly depends on the diameter of the rolls with respect to the thickness of the sheets and on the reduction per pass. The second component is introduced into the material by the friction existing between sheets and rolls: the shear acts in ND plane in RD direction. Friction is even more important in ARB than in conventional rolling, as the sheared surface layers are placed in the sheet interior by stacking for subsequent ARB rolling cycles and probably do not get totally overprinted by plane strain deformation. Therefore, a through-thickness strain gradient arises that may result in different rates of microstructure evolution along the thickness of the sample [7] leading to a heterogeneous microstructure and texture. As a consequence, anisotropy of the so-processed sheets can have different origins: textures and microstructural features as well as their through-thickness heterogeneities. To characterize the plastic anisotropy of metal sheets the Lankford parameter [8] is an important quantity. In the case of deep drawing, for example, the Lankford parameter can help to estimate the undesirable effects like thinning and earing.

Previously [9], the Lankford parameters were measured for ARB aluminium alloy AA6016 and simulated with the full and relaxed constraints Taylor theory [10–12] using an approach based on the minimization of the Taylor factor as a function of strain mode [13–18]. As in a free tensile experiment because of an anisotropic plastic behaviour of metal sheets the contraction ratio q (strain in width to strain in tensile direction) is not 0.5, it was assumed that the true q value corresponds to a minimum of the required deformation work, i.e. to a minimum of the Taylor factor. In a similar investigation on conventionally rolled molybdenum sheets there was good agreement between the experimental Lankford parameters and those simulated according to this approach [19]. However, for the ARB aluminium alloy AA6016 this model strongly overestimates the plastic anisotropy [9]. The same discrepancy between experiment and simulation was also found by Park [20] for conven-

* Corresponding author. Fax: +33 3 87 31 53 66.
E-mail address: benoit.beausir@univ-metz.fr (B. Beausir).

0921-5093/$ – see front matter © 2010 Elsevier B.V. All rights reserved.
doi:10.1016/j.msea.2010.02.006

Table 1
Chemical composition of aluminium alloys AA1050 and AA6016 (wt.%).

	Si	Cu	Fe	Mn	Mg	Cr	Zn	Ti	Other	Al
AA1050	0.25	0.05	0.4	0.05	0.05	–	0.07	0.05	0.03	Balance
AA6016	1.0–1.5	0.2	0.5	0.2	0.25–0.5	0.1	0.2	0.15	0.15	Balance

tionally rolled aluminium alloy AA5052. Therefore, in the present work the experimental Lankford parameters of two ARB aluminium alloys (technical pure AA1050 and age-hardening AA6016) are compared with advanced bulk texture-based simulations using the viscoplastic self-consistent crystal plasticity model [21–23]. Effects of strain rate sensitivity, grain shape and slip system activity on the simulated anisotropies are discussed.

2. Experimental

The chemical composition of the aluminium alloys used is listed in Table 1. Sheets with different number of ARB cycles (initial 0, 2, 4, 6, 8) were produced according to the procedure described in detail in [24]. Sheets of AA1050 were ARB pocessed at room temperature, while those of AA6016 before each rolling cycle were pre-warmed to 230 °C for 4 min. After the last cycle the samples were air-cooled to room temperature.

The microstructure of the starting material and the ARB sheets was investigated with electron back scatter diffraction (EBSD) in a Zeiss Ultra 55 scanning electron microscope (SEM) equipped with a HKL EBSD system. The determination of the grain size was done via line intercept method considering only high angle grain boundaries (HAGBs) with misorientation angles larger than 15°. Its evolution with ARB cycles has already been published in detail elsewhere [24]. Therefore, here only a brief overview is given below.

The global textures (basis for anisotropy simulations, see below) were measured by neutron diffraction on a stack of eight sheets with a size of 10 mm × 10 mm. Because of their high penetration depth neutrons allow bulk texture measurements. The orientation distribution function (ODF) was calculated from the measured pole figures (200, 220, 111) using the harmonic method with a maximum series expansion coefficient of 22 [25,26]. The Euler angles used are in the Bunge notation [27]. Local textures were measured by EBSD in the Zeiss Ultra 55 SEM.

The tension tests were performed with a Zwick/Roell Z250 deformation machine at an initial strain rate of $9.2 \times 10^{-4}\,s^{-1}$ in air at room temperature. The tensile specimens had a dog bone shape. Due to the limited material available the length of the gauge section varied between 35 and 50 mm.

The optical system Aramis (GOM mbH, Germany) was used to register the strain within the sheets and measure the elongation (true tensile strain ε_x) and width contraction (true transverse strain ε_y) simultaneously. For this purpose, the sheet plane of the sample was covered statistically with a dot pattern which during the deformation was recorded by two cameras. The software Aramis splits the measuring surface into predetermined sections that can be identified by their characteristic dot pattern. The relative change of the position of the segments during the deformation is documented for every snap shot yielding $d\varepsilon_y$ and $d\varepsilon_x$ and hence r_α, which assuming volume constancy is given by

$$r_\alpha = \frac{d\varepsilon_{\text{width}}}{d\varepsilon_{\text{thickness}}} = \frac{d\varepsilon_y}{d\varepsilon_z} = -\frac{d\varepsilon_y}{d\varepsilon_x + d\varepsilon_y} = \frac{q}{1-q}. \quad (1)$$

with $q = -d\varepsilon_y/d\varepsilon_x$ being the contraction ratio.

The Lankford parameter depends on the direction of the sample within the sheet plane with α defining the angle between tensile axis and rolling direction (RD). As usual, the Lankford parameter in this work is measured at three angles $\alpha = (0°, 45°, 90°)$, and in the following will be referred to as r_{RD}, $r_{45°}$ and r_{TD} (TD = transverse direction).

From this orientation dependent Lankford parameter the mean Lankford parameter $\langle r \rangle$ and its variation Δr can be obtained characterizing the *average normal* and *planar anisotropy* of the whole sheet, respectively:

$$\langle r \rangle = \frac{1}{4}(r_{RD} + 2r_{45°} + r_{TD}), \quad (2)$$

$$\Delta r = \frac{1}{2}(r_{RD} - 2r_{45°} + r_{TD}). \quad (3)$$

With the help of these two parameters the mechanical anisotropy of the sheets can be quantified.

The Lankford parameter after a critical axial strain becomes constant. The ARB material used was ductile enough to reach the plateau value and this was taken for further discussion. In order to minimize the influence of local inhomogeneities at least three samples were taken from the same sheet and measured for each direction.

Based on the global texture of the sheets discretized into 2000 individual orientations, the Lankford parameters for different numbers of ARB cycles were simulated using the viscoplastic polycrystal self-consistent code developed by Lebensohn and Tomé [23] (VPSC, version 7b).

The dislocation density was assumed to increase with strain [28] and is believed to round the yield surface. This feature is indirectly taken into account in the simulations via the strain rate sensitivity index m of the viscoplastic flow law of Hutchinson [29] used in the present modelling. Relatively high strain rate sensitivity leads to the activation of more slip systems and also rounds the yield surface and thus can be interpreted as the effect of increasing the dislocation density in the material [30–33]. Three values of m were tested in this study: 0.2, 0.1 and 0.05.

Non-octahedral glide in fcc metals can play a significant role on the texture evolution during SPD (see Arzaghi et al. [33]). As a consequence, in the simulation of the Lankford parameter glide on $\{1\,0\,0\}\langle 1\,1\,0\rangle$ was added to the classical octahedral glide on $\{1\,1\,1\}\langle 1\,1\,0\rangle$ slip systems. A ratio p between the reference stresses of non-octahedral glide (τ^{NOC}) and octahedral glide (τ^{OC}) is defined by:

$$p = \frac{\tau^{NOC}}{\tau^{OC}}, \quad (4)$$

Four values of p were considered: 1, 1.25, 1.5 and $p > \sqrt{3}$, $\sqrt{3}$ being the critical value above which only octahedral glide is activated [33].

As shown in the next section, the coarse globular grain structure of the starting material during ARB changes into an ultrafine grained lamellar grain structure. With increasing number of ARB cycles the grains become elongated in the rolling direction. Therefore, the grain shape effect on the Lankford parameter was also tested by imposing an average aspect ratio (up to 10) with respect to the rolling direction of each grain constituting the texture after ARB. However, the impact of the grain shape was negligible compared to the effects of the strain-rate sensitivity index or of the ratio p and so spherical initial grain shapes were selected.

3. Results and discussion

During ARB the coarse globular grain structure of the starting material changes to an ultrafine grained lamellar structure. BSE images of both alloys (Fig. 1) show that the grains are clearly elongated in the rolling direction. Thus, the grain size in rolling direction (d_{RD}) can be distinguished from that in normal direction (d_{ND}). Table 2 lists the average grain sizes for both alloys as a function

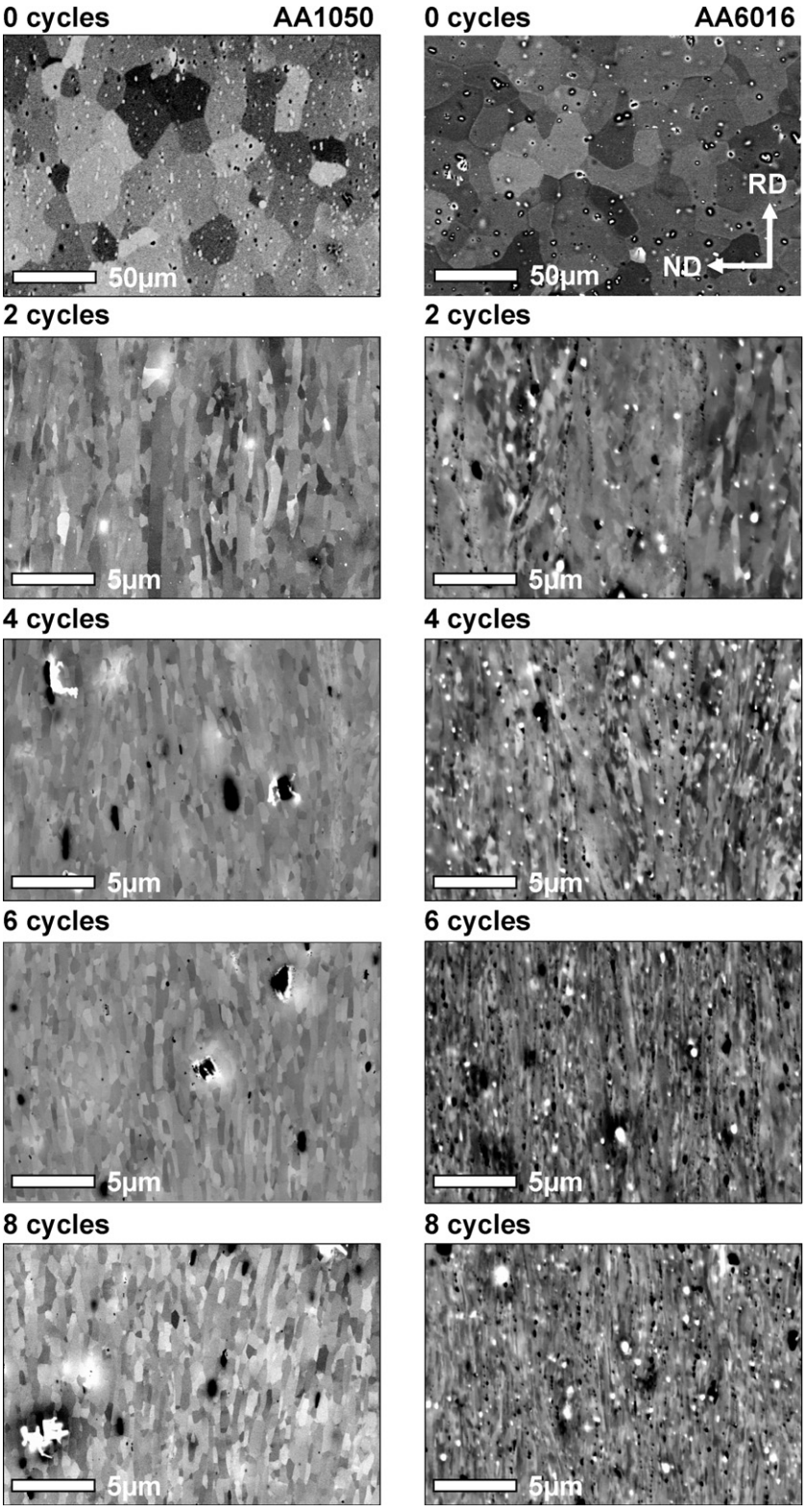

Fig. 1. BSE images of the grain structure in ARB sheets after 0, 2, 4, 6 and 8 cycles for AA1050 and AA6016 in the TD plane.

of the number ARB cycles. For both alloys an important grain size reduction was observed after 2 cycles. However, for the subsequent cycles the grain size remained about constant in AA1050 while in AA6016 the grain size slightly decreased up to 8 cycles.

Fig. 2 shows the texture after 0, 4 and 8 ARB cycles in both alloys displayed as ODF sections at $\varphi_2 = 45^\circ$. The texture of the initial recrystallized state in AA6016 consists of a strong cube and a minor Goss component, while in AA1050 the cube component is strongly predominant with respect to a small Goss and copper component. During ARB this texture rapidly changes to a typical rolling texture of face-centered cubic metals with a major copper and minor brass component for both materials. Moreover, the rotated cube

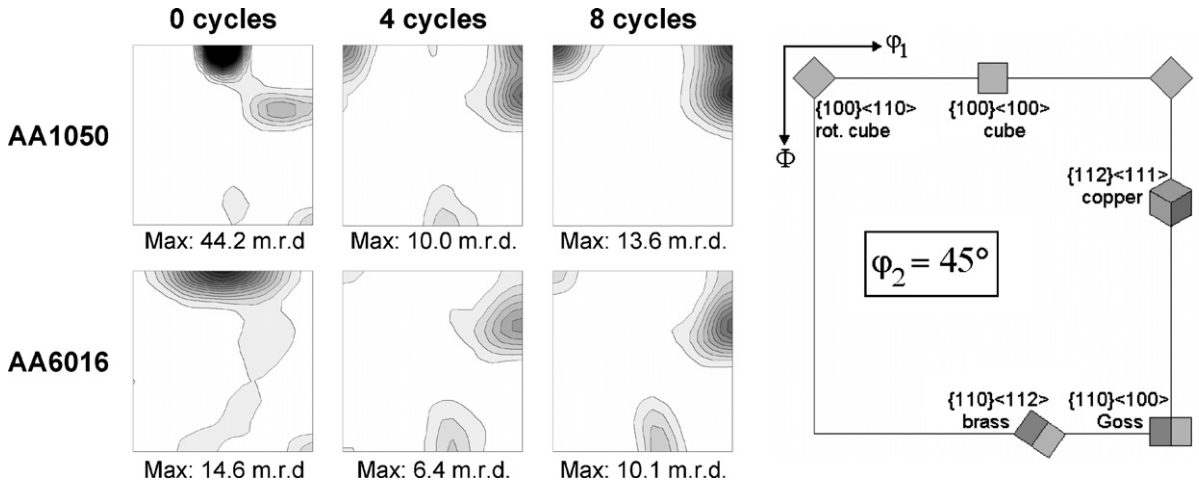

Fig. 2. Texture after 0, 4 and 8 ARB cycles in AA1050 and AA6016 displayed as ODF sections at $\varphi_2 = 45^\circ$ with intensities given in multiples of a random distribution (m.r.d.). The key figure shows the position of the main texture components.

component, which represents a typical shear component, namely *C* component [30,34], forms in both alloys with higher intensity in AA1050. The development of the rotated cube component by shearing is favoured by the initial cube texture of the starting material [35]. As revealed by preliminary local texture measurements, the shear component mainly exists in a thin surface layer of the ARB stack. A detailed characterization of the local texture is under way.

Fig. 3 for the two alloys presents the evolution of the Lankford parameters for three directions as well as the average normal and planar anisotropy as a function of the number of ARB cycles. The evolution of these parameters as a function of the number of cycles is comparable for both alloys: r_{45° values strongly increase with the number of ARB cycles while r_{RD} and r_{TD} both decrease. In the initial state r_{RD} and r_{TD} are higher than r_{45°. After two ARB cycles this relation is reversed. Differences between the two alloys decrease with the number of cycles. They are more pronounced up to 4 cycles, at 6 and 8 cycles they are minimum. It is most interesting to compare the value of r_{45° for both alloys. The alloy with a stronger shear texture component (AA1050) up to four cycles presents a lower r_{45° value. However, at larger number of cycles (6 and 8) r_{45° becomes comparable in both alloys.

The average normal anisotropy $< r >$ increases steadily with increasing number of ARB cycles from about 0.6 to 0.9 for both materials. The average planar anisotropy Δr decreases and changes sign (from about 0.6 to −0.7 for AA050 and 0.2 to −0.7 for AA6016), shifting earing from the RD/TD positions ($\Delta r > 0$) in the initial state to the 45° positions ($\Delta r < 0$) in the 'high-cycle' ARB state. Regarding the deep drawing properties the evolution of $< r >$ and Δr is contrasting. A large value of the average normal anisotropy $< r > \gg 1$ reduces thinning of the walls. For minimal earing a planar anisotropy $\Delta r \approx 0$ is desirable. Thus, for good deep drawing conditions r_α should be large and comparable for all directions. According to experiment the best conditions for deep drawing are fulfilled for 'low-cycle' ARB.

In the following experimental and calculated Lankford parameters will be compared and discussed. As can be seen in Figs. 4 and 5, in general for both aluminium alloys the simulated Lankford parameters with respect to the number of ARB cycles show the same trend as those experimentally measured. The Lankford

Table 2
Average grain sizes of aluminium alloys AA1050 and AA6016 as function of the number ARB cycles.

Cycles	AA1050		AA6016	
	d_{RD} (μm)	d_{ND} (μm)	d_{RD} (μm)	d_{ND} (μm)
0	22.62	13.50	18.20	16.19
2	1.16	0.79	1.85	1.37
4	0.85	0.46	0.74	0.58
6	0.82	0.50	0.56	0.30
8	0.96	0.52	0.47	0.21

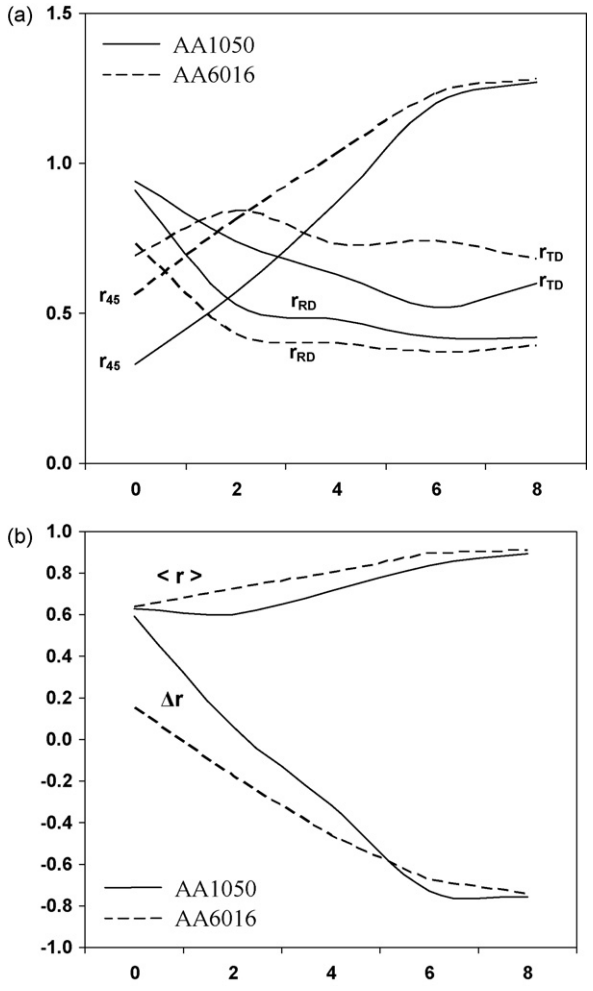

Fig. 3. Comparison of in-plane plastic anisotropy of AA1050 and AA6016 alloys.

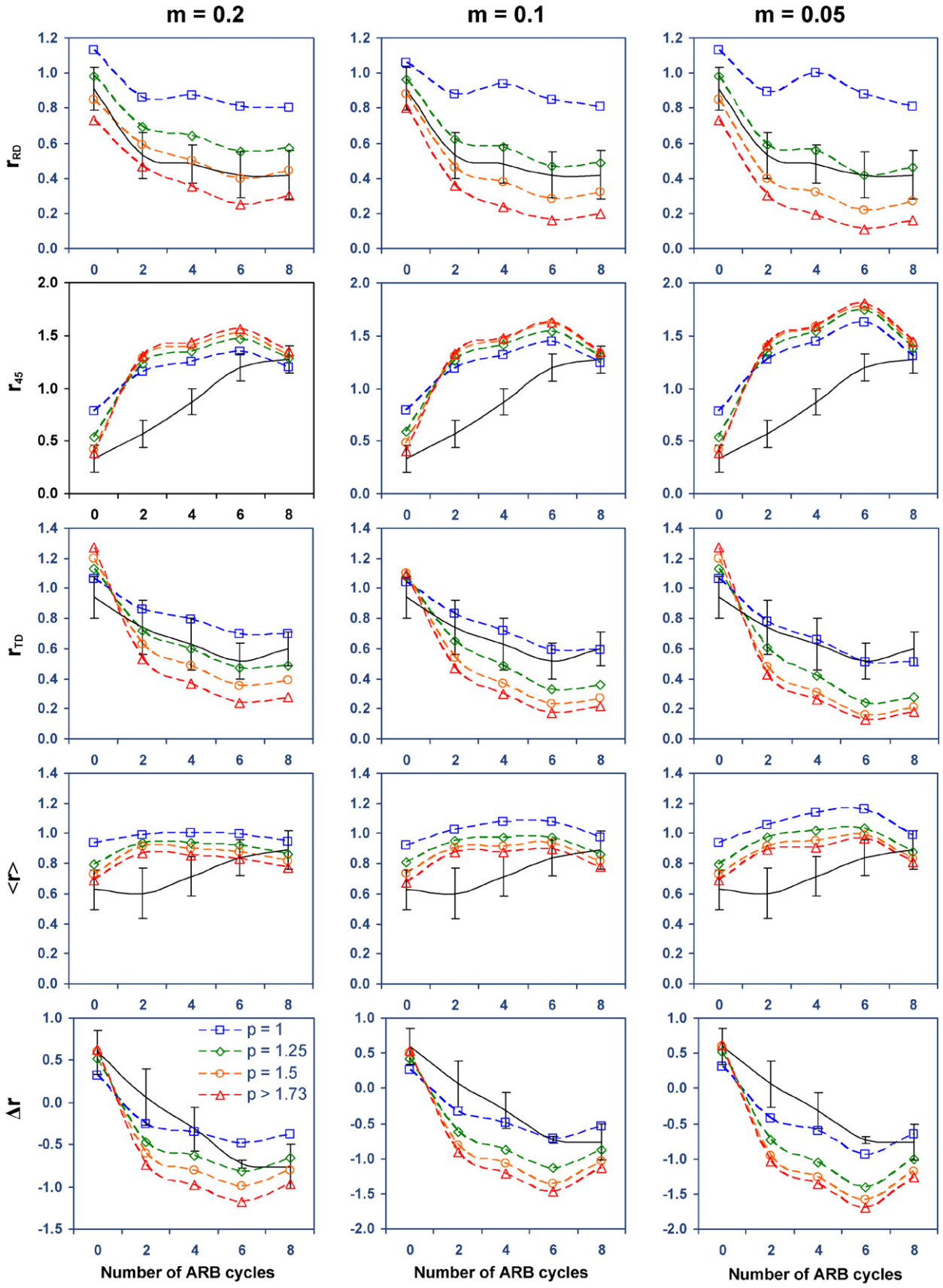

Fig. 4. Measured (solid lines) and simulated (broken lines) anisotropy parameters (Lankford parameter r, average normal anisotropy $\langle r \rangle$ and planar anisotropy Δr) of AA1050 as a function of the number of ARB cycles for different strain rate sensitivity m and activity of non-octahedral slip p.

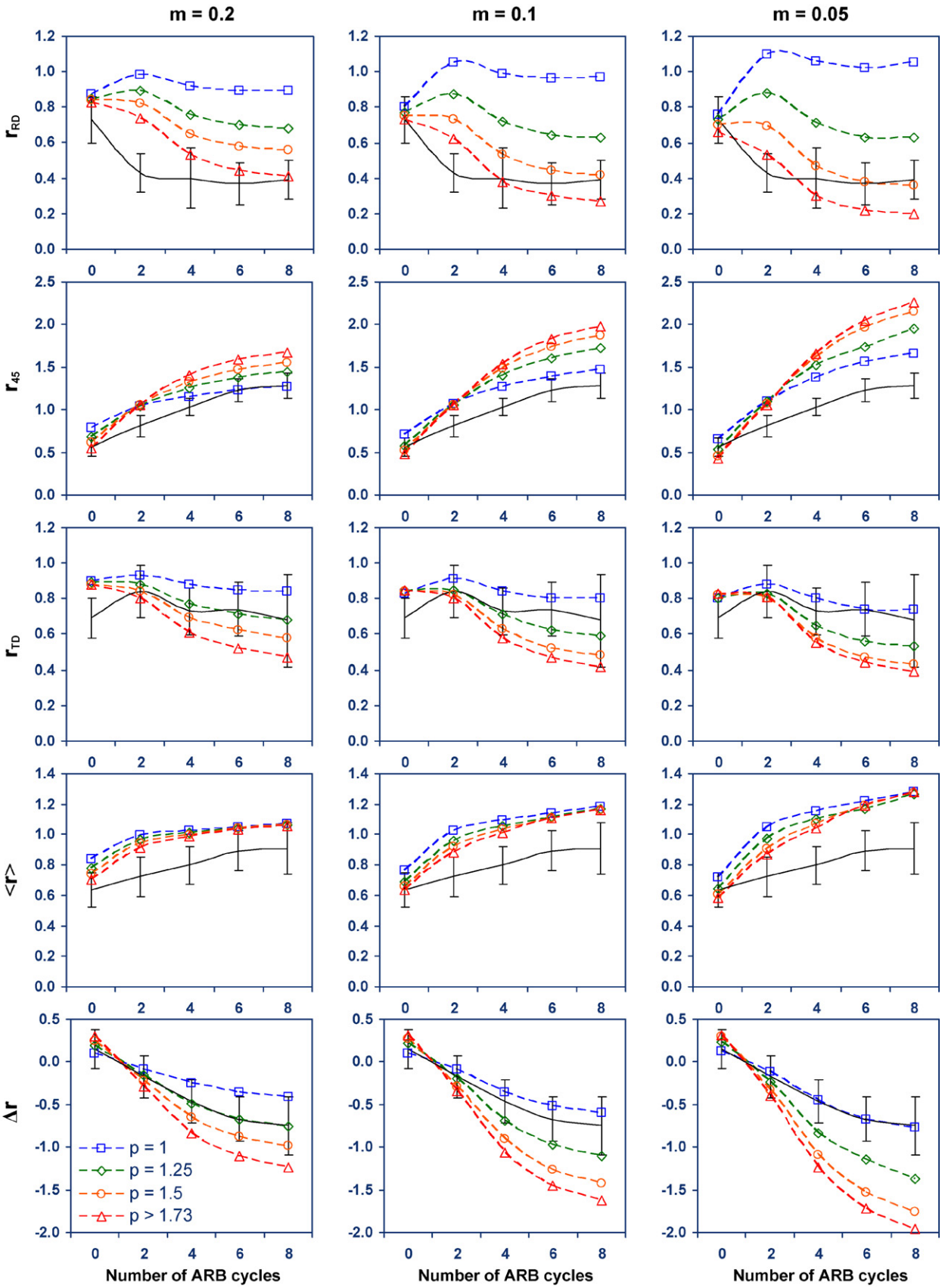

Fig. 5. Measured (solid lines) and simulated (broken lines) anisotropy parameters (Lankford parameter r, average normal anisotropy $\langle r \rangle$ and planar anisotropy Δr) of AA6016 as a function of the number of ARB cycles for different strain rate sensitivity m and activity of non-octahedral slip p.

parameters r_{RD} and r_{TD} increase with the activity of the non-octahedral slip systems, on the contrary $r_{45°}$ decreases. A similar effect is obtained by increasing the strain rate sensitivity: r_{RD} and r_{TD} increases while $r_{45°}$ decreases. Indeed, increasing strain rate sensitivity contributes to the activation of more slip systems [30–33]. Thus, this effect works in the same way as adding non-octahedral slip systems. Although it is physically reasonable to consider that the strain-rate sensitivity index as well as the contribution of non-octahedral glide can evolve with the number of ARB cycles, globally a good agreement between simulation and experiment was obtained for $m = 0.2$ and $p = 1.25$. Under these conditions, depending on the α angle and the number of ARB cycles, the activity of the non-octahedral slip systems represents between 15 and 35% of the total glide during the simulated tensile tests.

Even if the simulated average normal anisotropy remains within the experimental error $\langle r \rangle_{exp}$ is smaller than $\langle r \rangle_{sim}$ leading to more wall thinning than the simulations predict. On the other hand, the experimental Lankford parameters for different directions (Figs. 4 and 5) do not differ as much from each other as in the simulations and therefore Δr is much smaller reducing earing.

While r_{RD} and r_{TD} are globally always quite well reproduced by the simulation, an interesting point is that for both materials $r_{45°}$ seems always overestimated, in particular in the case of AA1050.

For AA1050 (see Fig. 4), the alloy presenting the stronger shear component, an important overestimation of $r_{45°}$ by the simulation can be observed. This overestimation increases and is maximum for 2 and 4 ARB cycles, then decreases for 6 cycles and finally becomes near zero for 8 cycles. In the case of AA6016 (see Fig. 5), the alloy displaying less shear component, it can be seen that the simulations also overestimate $r_{45°}$ and especially for 2 and 4 ARB cycles, but the overestimation is clearly smaller than for AA1050. This suggests that the strength of the shear texture component is somehow responsible for it.

To investigate the effect of the two main texture components on the plastic anisotropy, three model textures have been artificially produced: rotated cube component due to the shear produced by friction between the rolls and the surface of the sheet, copper component resulting from plane strain deformation and finally a combination (with equal intensity) of both components. Lankford parameters simulated with these three model textures are presented in Fig. 6. One can see that for the copper component $r_{45°}$ is smaller than r_{RD} and r_{TD} while for the rotated cube component the situation is reversed. Interestingly, when the texture is composed of both components the simulated Lankford parameter clearly follows the trend of the rotated cube component taking only. The same values of r_{RD} and r_{TD} are obtained in the two cases (both components and rotated cube only) while $r_{45°}$ becomes larger when the two components are taken together. The main point of this result is the fact that the simulated $r_{45°}$ is about the same for a texture composed by the copper component and a texture composed by both rotated cube and copper component.

If we go back now to the experimental results, the texture of AA1050 is composed by both components (rotated cube and copper) while AA6016 is composed by mostly the copper component (see Fig. 2). As a consequence, according to the simulation results on these artificially made textures, the experimental $r_{45°}$ should be comparable. If we compare the $r_{45°}$ values for the two alloys it is only true from 6 cycles on (see Fig. 3a). Moreover, as discussed before, the worst results of simulation are for $r_{45°}$ and for 2 and 4 cycles and even for the more sheared alloy (AA1050).

In the first pass of rolling, the shear components produced by friction between the rolls and the sheet were found in the surface layers. During subsequent ARB cycles due to the bonding process the surface shear texture is put in the middle of the sheet, generating heterogeneities of texture through the thickness of the sheet (strong shear component in the surface layers and in the center, while the texture of the rest is mainly a texture of plain strain compression). With more ARB bonding, the shear texture component will be present through the bulk of the sheet and thus the texture heterogeneity decreases. Indeed, from local texture measurements of the first cycle (not presented here), for both materials only the surface layers of the sheets produced by ARB contain a significant amount of rotated cube component ($\{1\,0\,0\}\langle 1\,1\,0\rangle$). This component becomes comparable in intensity with the copper component when the global texture is measured, although it appears only in thin layers close to the surfaces of the sheets.

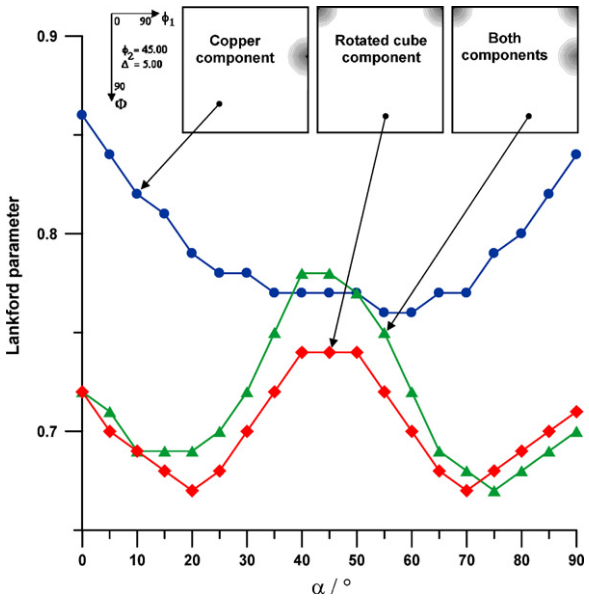

Fig. 6. Simulated Lankford parameter (for $m = 0.2$ and $p = 1.25$) as function of α (angle between tensile axis and rolling direction) for the copper component, rotated cube component and a superposition of both. Maximum ODF intensities of all components are 6 m.r.d.

As a consequence, by using the global texture measurements, which do not reflect the spatial distribution of the components through the thickness of the sheet, as input texture for the simulations, the Lankford parameters are less well reproduced when the heterogeneity is important, i.e. up to about four cycles.

To summarize, when the shear texture component is strong (here AA1050) the texture heterogeneity becomes important and the simulation results based on the global texture measurements become less satisfying, and especially for small number of ARB cycles where the heterogeneity is maximum. The lower shear texture component existing in the AA6016 alloy produces less texture heterogeneities through the thickness. As a consequence, the overestimation of $r_{45°}$ by the simulations is lower (compare Figs. 4 and 5).

Therefore, it remains a future issue to determine with detailed local texture measurements the thickness of the surface layer affected by shear and treat the ARB material with regard to texture as a layered composite. Another possible way should be to perform simulations of the texture evolution during ARB and use the so-obtained simulated texture as input for Lankford parameter simulations. A model based on the description on the material flow via analytical flow line function is in progress. Such a modelling is able to take into account the position of a material flow element through the thickness of the sheet [36].

4. Concluding remarks

Measurements of the Lankford parameter show that the plastic anisotropy of the ultrafine grained aluminium alloys AA1050 and AA6016 changes with the number of ARB cycles. This trend can be simulated well with the viscoplastic polycrystal self-consistent model taking into account the global texture, strain rate sensitivity, non-octahedral slip and grain shape. However, deviations between experiment and simulation are quite important for the first ARB cycles and especially at 45° to the rolling direction. According to the present results and observations, these deviations could be attributed to the fact that the present modelling as well as the neutron diffraction texture measurements are not able to account for the spatial distribution of the texture components through the thickness. Therefore, the quality of the simulation results is low (and especially for r_{45°) when through thickness texture heterogeneity is important, i.e. when the friction between the rolls and the sheet give an important shear texture component (like here for AA1050), and/or for the first ARB cycles when the shear component is not already "mixed" by several bondings.

Acknowledgments

The ARB aluminium samples were kindly provided by Dr. H.W. Höppel, University Erlangen-Nürnberg. Sample preparation of T. Reiter is gratefully acknowledged. B. Beausir is grateful to the Alexander von Humboldt Foundation for his research fellowship.

References

[1] C.C. Koch, in: M.J. Zehetbauer, Y.T. Zhu (Eds.), Bulk Nanostructured Materials, WILEY-VCH Verlag GmbH & Co. KGaA, Weinheim, 2009, pp. 3–20.
[2] R.Z. Valiev, A.A. Nazarov, in: M.J. Zehetbauer, Y.T. Zhu (Eds.), Bulk Nanostructured Materials, WILEY-VCH Verlag GmbH & Co. KGaA, Weinheim, 2009, pp. 21–48.
[3] H. Pirgazi, A. Akbarzadeh, R. Petrov, L. Kestens, Materials Science and Engineering A—Structural Materials Properties Microstructure and Processing 497 (2008) 132–138.
[4] H. Pirgazi, A. Akbarzadeh, R. Petrov, J. Sidor, L. Kestens, Materials Science and Engineering A—Structural Materials Properties Microstructure and Processing 492 (2008) 110–117.
[5] S.G. Chowdhury, V.C. Srivastava, B. Ravikumar, S. Soren, Scripta Materialia 54 (2006) 1691–1696.
[6] N. Tsuji, in: M.J. Zehetbauer, Y.T. Zhu (Eds.), Bulk Nanostructured Materials, WILEY-VCH Verlag GmbH & Co. KGaA, Weinheim, 2009, pp. 235–253.
[7] N. Tsuji, Y. Saito, S.H. Lee, Y. Minamino, Proceedings of the Conference Nanomaterials by Severe Plastic Deformation—NANOSPD2, Vienna, Austria, December 9–13, 2002.
[8] W.F. Lankford, S.C. Snider, J.A. Bausch, Transactions American Society of Metals 42 (1950) 1197–1232.
[9] W. Skrotzki, I. Hünsche, J. Hüttenrauch, C.-G. Oertel, H.G. Brokmeier, H.W. Höppel, Topic, Texture, Stress, and Microstructure (2008), doi:10.1155/2008/328754, 9 pp.
[10] G.I. Taylor, Journal of the Institute of Metals 62 (1938) 307–324.
[11] J.F.W. Bishop, R. Hill, Philosophical Magazine 42 (1951) 414–427.
[12] J.F.W. Bishop, R. Hill, Philosophical Magazine 42 (1951) 1298–1307.
[13] W.F. Hosford, The Mechanics of Crystals and Textured Polycrystals, Oxford University Press, New York, 1993, pp. 56–102.
[14] P. van Houtte, Textures and Microstructures 8–9 (1988) 313–350.
[15] M. Heilmaier, M. Nganbe, B. Beckers, H.-G. Brokmeier, R. Tamm, C.-G. Oertel, W. Skrotzki, Materials Science and Engineering A—Structural Materials Properties Microstructure and Processing 319–321 (2001) 290–293.
[16] H.J. Bunge, Kristall und Technik 5 (1970) 145–175.
[17] P. van Houtte, Material Science Forum 273–275 (1998) 67–76.
[18] W. Skrotzki, R. Tamm, C.-G. Oertel, B. Beckers, H.-G. Brokmeier, E. Rybacki, Materials Science and Engineering A—Structural Materials Properties Microstructure and Processing 319–321 (2001) 364–367.
[19] C.-G. Oertel, I. Hünsche, W. Skrotzki, W. Knabl, A. Lorich, J. Resch, Materials Science and Engineering A—Structural Materials Properties Microstructure and Processing 483–484 (2008) 79–83.
[20] J.J. Park, Journal of Materials Processing Technology 87 (1999) 146–153.
[21] R. Hill, Journal of Mechanics and Physics of Solids 13 (1965) 89–101.
[22] A. Molinari, G.R. Canova, S. Ahzi, Acta Metallurgica 35 (1987) 2983–2994.
[23] R.A. Lebensohn, C.N. Tomé, Acta Metallurgica et Materialia 41 (1993) 2611–2624.
[24] J. Scharnweber, W. Skrotzki, C.-G. Oertel, H.-G. Brokmeier, H. W. Höppel, Topic, Advanced Engineering Materials (2010).
[25] M. Dahms, H.J. Bunge, Journal of Applied Crystallography 22 (1989) 439–447.
[26] M. Dahms, T. Eschner, Quantitative Texturanalyse durch iterative Reihenzerlegung von Beugungs-Polfiguren (Software Manual), 1996.
[27] H.-J. Bunge, Zeitschrift für Metallkunde 56 (1965) 872–874.
[28] P. Les, M. Zehetbauer, H.P. Stuwe, Physica Status Solidi A—Applied Research 157 (1996) 265–273.
[29] J.W. Hutchinson, Proceedings of the Royal Society of London A 348 (1976) 101–127.
[30] L.S. Tóth, P. Gilormini, J.J. Jonas, Acta Metallurgica 36 (1988) 3077–3091.
[31] L.S. Tóth, F. Qods, J.-J. Fundenberger, Zeitschrift für Metallkunde 96 (2005) 1038–1043.
[32] B. Beausir, L.S. Tóth, K.W. Neale, International Journal of Plasticity 23 (2007) 227–243.
[33] M. Arzaghi, B. Beausir, L.S. Tóth, Acta Materialia 57 (2009) 2440–2453.
[34] U.F. Kocks, G.R. Canova, J.J. Jonas, Acta Metallurgica 31 (1983) 1243–1252.
[35] W. Skrotzki, N. Scheerbaum, C.-G. Oertel, H.-G. Brokmeier, S. Suwas, L.S. Tóth, Materials Science Forum 503–504 (2006) 99–106.
[36] B. Beausir, L.S. Tóth, O. Bouaziz, Materials Science Forum 496–497 (2005) 1603–1608.